Computation of the Force Density inside the Channel of an Electromagnetic Pump Using Hermite Projection

N. Takorabet

Computation of the Force Density inside the Channel of an Electromagnetic Pump Using Hermite Projection

N. TAKORABET, IEEE member

***Abstract*-- The paper presents a coupled model of linear induction pump for liquid metal. The magnetic filed in the motionless domains is computed by finite elements analysis while the filed inside the moving parts are computed by Fourier transform and spectral decomposition on Hermite basis. The paper is focused on the analysis of the force density according to the current supply and speed variations.**

***Index Terms*-- eddy currents, finite element methods, linear induction pumps, force density, Hermite functions**

I. INTRODUCTION

In the industrial processes dealing with molten metals, electromagnetic devices are used to move liquid metal such as aluminum or sodium. Linear induction pumps are devices creating sliding waves inducing currents inside the liquid metal that is moved thanks to the forces created by the induction phenomenon [1]. If finite element method is adopted, the main difficulty encountered when simulating such devices is caused by the convective terms $\boldsymbol{v}\times\boldsymbol{B}$ due to the movement, where $\boldsymbol{B}$ is the flux density and $\boldsymbol{v}$ is the velocity. This difficulty can be avoided by using some techniques that are very efficient in the case of rotating induction motors where a discrete spectrum of space harmonics is in presence [2, 3, 4]. However, these methods are not adapted for linear induction motor which is characterized by a continuous spectrum of space harmonics. A combined method using Fourier and transform finite elements analysis leads to introduce a convolution relation between the magnetic vector potential and its normal derivative on the boundary of the moving parts is developed and tested [5]. This method allows computing the electromagnetic field distribution in the motionless parts of the device by Hermite spectral decomposition. Indeed, the projection on orthogonal basis of Hermite functions allows computing simultaneously the fields and their Fourier transform. The external performances of the linear pump can be computed as quadratic forms of the supply currents. Then an optimization process can be performed to define the optimal supply currents satisfying a given criterion [6]. For this purpose, the field inside the moving parts is not computed and all the numerical computations are performed in the motionless parts of the device.

The aim of this paper is to compute the force density field inside the moving parts and to analyze it when the supply is modified. Thanks to the projection on the Hermite orthogonal basis, the computation of the output mechanical power is achieved with a simplified expression.

N. Takorabet is with Groupe de Recherche en Electrotechnique et Electronique de Nancy – INPL – CNRS (UMR 7037), 02 avenue de la forêt de Haye 54516 Vandoeuvre-lès-Nancy FRANCE (telephone: +33(0)383595657 e-mail: noureddine.takorabet@ensem.inpl-nancy.fr).

II. ELECTROMAGNETIC MODEL

In a 2D approximation, we can use a magnetic vector potential (mvp) owning one component in the z-direction while Fig. 1 shows a cross section of the device in the (x-y) plan. The motionless domain contains the stator armature and the air while the moving domain D of boundary ∂D, is the liquid metal. This later, of a thickness 2α, present an electric conductivity σ and a magnetic permeability μ. The air gap, of thickness β, is made of ceramic owning electromagnetic characteristics close to those of the air and gives an efficient thermal insulation. Thanks to the symmetry, only half a device is represented. The power supply is sinusoidal and the saturation of ferromagnetic materials is not taken into account so a complex representation $\overline{G}(x,y)$ of sinusoidal quantities $g(x,y,t)$ is adopted. Indeed, the large air-gap leads to have weak values of the flux density in the iron, so it is never saturated. More, the domain D is invariant along the direction of the movement so it does not generate additional time harmonics.

In this study the liquid metal is considered homogenous with a constant speed $\boldsymbol{v}$ along the x-direction. The speed variation

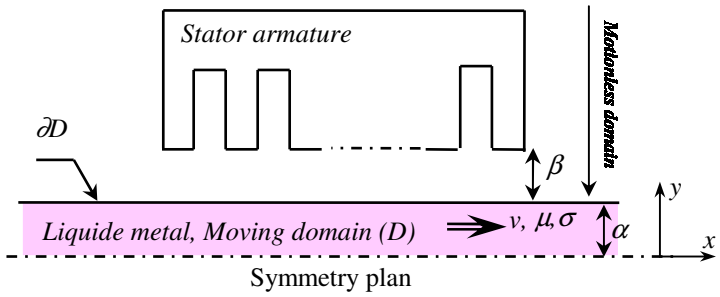

Fig. 1. Definition of the domains and their properties

along the viscous boundary layer is neglected. Because of the no periodicity of the structure, Fourier transform $\hat{A}(k,y)$ of the magnetic vector potential (mvp) $\overline{A}(x,y)$ is introduced. Since $\overline{A} \in L^2(D)$, we have :

$$\hat{A}(k,y) = \int_R \overline{A}(x,y)\exp(-2j\pi kx)dx \tag{1}$$

and reciprocally,

$$\overline{A}(k,y) = \int_R \hat{A}(k,y)\exp(+2j\pi kx)dk \tag{2}$$

The mvp inside the domain D is governed by:

$$\frac{\partial^2\overline{A}}{\partial x^2} + \frac{\partial^2\overline{A}}{\partial y^2} = j\mu\sigma(\omega\overline{A} + v\frac{\partial\overline{A}}{\partial x}) \qquad \text{in } D \tag{3}$$

with : $\partial\overline{A}/\partial y = 0$ on $y = 0$

Using the Fourier transform, these problem can be written :

$$\frac{\partial^2\hat{A}}{\partial y^2} = \varphi^2(k)\hat{A} \qquad \text{in } D \tag{4}$$

with: $\partial\hat{A}/\partial y = 0$ on $y = 0$

and: $\varphi^2(k) = 4\pi^2k^2 + j\omega\mu\sigma(1 + kv/f)$

The solution of such equation is of the form :

$$\hat{A}(k,y) = C_1\cosh[\varphi(k)y] \tag{5}$$

where C_1 is a constant.

Resolving this equation one can determine that $\hat{A}$ on the boundary ∂D and its normal derivative are linked by :

$$\frac{\partial\hat{A}}{\partial y}(k,\alpha) = \hat{g}(k)\hat{A}(k,\alpha) \tag{6}$$

where: $\hat{g}(k) = (\mu_0/\mu)\,\varphi(k)\tanh[\varphi(k)]$

So we have :

$$-\frac{\partial\overline{A}}{\partial y}(x,\alpha) = \int_R g(u)\overline{A}(x-u,\alpha)du \tag{7}$$

This convolution is introduced in a finite elements analysis by using a projection on the basis of Hermite functions Ψ_n. In fact, Ψ_n functions are obtained from Hermite orthogonal polynomials and present the property of being invariant with respect to Fourier transform.

$$\hat{\psi}_n(k) = \int_R \psi_n(k)\exp(-2j\pi kx)dx = (-j)^n\psi_n(k) \tag{8}$$

Under the hypothesis of linear magnetization curve *b(h)* of ferromagnetic materials, a superposition principle is applied. It consists in solving two groups of elementary problems and obtain elementary fields that are combined with the convolution (7) to obtain the coupling of the final solution in the motionless domain. In the first group, the mvp on the boundary ∂D is set to zero while the slots are supplied with unit current supply. In the second group, the slots are currentless while the mvp on ∂D is $\overline{A}(x,\alpha) = \psi_n(x)$, $n = 0,1,...N$. N is the order of the approximation of the mvp on the Hermite basis. The details of the method are well described in [5, 6]. After resolution, the mvp is determined in the motionless domain an in particular, on the boundary ∂D . It is of the form:

$$\overline{A}(x,\alpha) = \sum_{n=0}^{N}\overline{\alpha}_n\psi_n(x) \tag{9}$$

Using the property of the ψ_n with respect to Fourier transform, we can write :

$$\hat{A}(k,\alpha) = \sum_{n=0}^{N}\overline{\alpha}_n\hat{\psi}_n(k) \tag{10}$$

So using (10) and (5) one can determine the Fourier transform of the mvp at any level $y = y_i \in [0,\alpha]$ inside the secondary.

$$\hat{A}(k,y_i) = \sum_{n=0}^{N}\overline{\alpha}_n\hat{\psi}_n\frac{\cosh[\varphi(k)y_i]}{\cosh[\varphi(k)\alpha]} \tag{11}$$

Thanks to the properties of the chosen basis, we have:

$$\overline{A}(x,y_i) = \sum_{m=0}^{N}\overline{\alpha}_m^i\psi_m(x) \tag{12}$$

where: $\overline{\alpha}_m^i = \sum_{n=0}^{N}\overline{\alpha}_n\int_R \frac{\cosh[\varphi(k)y_i]}{\cosh[\varphi(k)\alpha]}\hat{\psi}_n(k)\hat{\psi}_m^*(k)dk$ (13)

By this way, the mvp inside the secondary is determined at different layers $y = y_i$ by its spectral decomposition on the Hermite basis. So if a regular mesh is performed on the secondary that coincides on the different layers, the mvp can be determined and drown anywhere in the device :

- by FE analysis in the motionless domain
- by (12) in the moving domain.

The flux lines are drown using the connected meshes and shown on Fig. 2. One can clearly see that the fields are well connected and the boundary conditions on ∂D are well respected. The effect on the velocity is observed by the deformation of the lines in the direction of the movement.

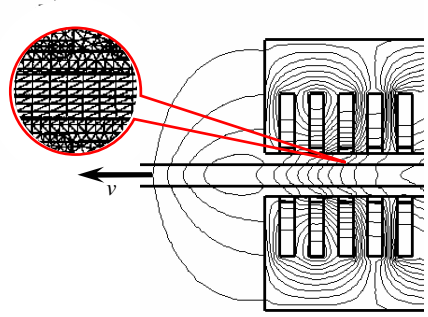

Fig. 2. Connecting flux lines between moving and montionless domains.

III. COMPUTATION OF THE FORCE DENSITY

The current density inside the secondary is given by:

$$\boldsymbol{J} = \sigma\left[j\omega\boldsymbol{A} + \boldsymbol{v}\times(\nabla\times\boldsymbol{A})\right] \tag{14}$$

The mean value of the force density inside the secondary is :

$$\boldsymbol{F} = \boldsymbol{J}\times(\nabla\times\boldsymbol{A}) \tag{15}$$

The pulsating component of the force density is not taken into account in (15). Its effect on the power conversion is negligible since the period of pulsations is too small compared to the typical time scale of the motion of the liquid metal. Projecting (15) on the (*x*-*y*) axes, the two components f_x and f_y are:

$$\begin{aligned} f_x &= \sigma\omega\Im\left[\overline{A}\frac{\partial\overline{A}^*}{\partial x}\right] - \sigma v\left|\frac{\partial\overline{A}}{\partial x}\right|^2 \\ f_y &= \sigma\omega\Im\left[\overline{A}\frac{\partial\overline{A}^*}{\partial y}\right] - \sigma v\,\Re\left[\frac{\partial\overline{A}}{\partial x}\frac{\partial\overline{A}^*}{\partial y}\right] \end{aligned} \tag{16}$$

where $\Re$ and $\Im$ mean "real part" and "imaginary part" respectively. Equations (16) are then projected on Hermite basis and expressed at different layers $y = y_i$ to obtain :

$$\begin{aligned} f_x(x,y_i) &= \sigma\sum_{n,m=0}^{N}\psi_n(x)\psi_m(x)\left[\omega\Im\left(\overline{\alpha}_n^i\overline{\gamma}_m^{i\,*}\right) - \sigma\left(\overline{\gamma}_n^i\overline{\gamma}_m^{i\,*}\right)\right] \\ f_y(x,y_i) &= \sigma\sum_{n,m=0}^{N}\psi_n(x)\psi_m(x)\left[\omega\Im\left(\overline{\alpha}_n^i\overline{\beta}_m^{i\,*}\right) - \sigma\,\Re\left(\overline{\gamma}_n^i\overline{\beta}_m^{i\,*}\right)\right] \end{aligned} \tag{17}$$

with :

$$\begin{aligned} \overline{\beta}_n^i &= \sum_{m=0}^{N}\overline{\alpha}_m\int_R \varphi(k)\frac{\sinh[\varphi(k)\,y_i]}{\cosh[\varphi(k)\,a]}\,\hat{\psi}_n(k)\,\psi_m^*(k)\,dk \\ \overline{\gamma}_n^i &= \sum_{m=0}^{N}\overline{\alpha}_m\int_R 2j\pi k\frac{\cosh[\varphi(k)\,y_i]}{\cosh[\varphi(k)\,a]}\,\hat{\psi}_n(k)\,\psi_m^*(k)\,dk \end{aligned} \tag{18}$$

As the coefficients $\overline{\alpha}_n^i$, that are given by (13), the coefficients $\overline{\beta}_m^i$ and $\overline{\gamma}_m^i$ are deduced from the spectral decomposition of the mvp on the boundary ∂D thanks to the orthogonality of the ψ_n functions. These coefficients correspond to the projection of the derivatives $\partial\widehat{A}/\partial x$ and $\partial\widehat{A}/\partial y$ of the mvp on the Hermite basis.

The case of linear pump with 18 slots stator armature is studied. The stator double layers winding is made up with 13 coils of a 5 slots pitch (Fig. 3). The optimization process is performed in the motionless domain to determine the 13 currents maximizing the force as well presented in [5] for $v = 0$. Using this optimal distribution of the currents, the force field is computed by (17) and shown in Fig. 4 through the tow components f_x and f_y. The f_x components presents a regular shape almost constant in the *y*-direction and decreases slightly at the extremities of the device. In all the following figures, the channel is zoomed in the *y*-direction. The f_y component presents an anti-symmetric shape in the *y*-direction. A vectorial visualization of the force field is presented in Fig. 5. It shows that the liquid metal is compressed in the *y*-direction while it is moved in the *x*-direction. An interesting conclusion is that the optimization process leads to a quite regular force field especially in the *x*-direction. A symmetry with respect to the axis $x = 0$ of the force fields are obtained because there is no movement of the fluid ($v = 0$). If the same process is performed at a non zero speed, the force distribution is modified by the movement. Figure 6 shows the f_x component for two values of the relative speed v_r which is the ratio of the speed v and a reference speed. The fore density field is translated in the direction of the movement and some perturbations appears. Another way to analyze the force density consists in performing the Hodge-Helmholtz

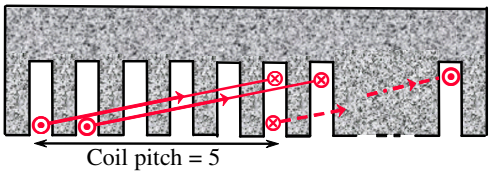

Fig. 3. Representation of the stator winding

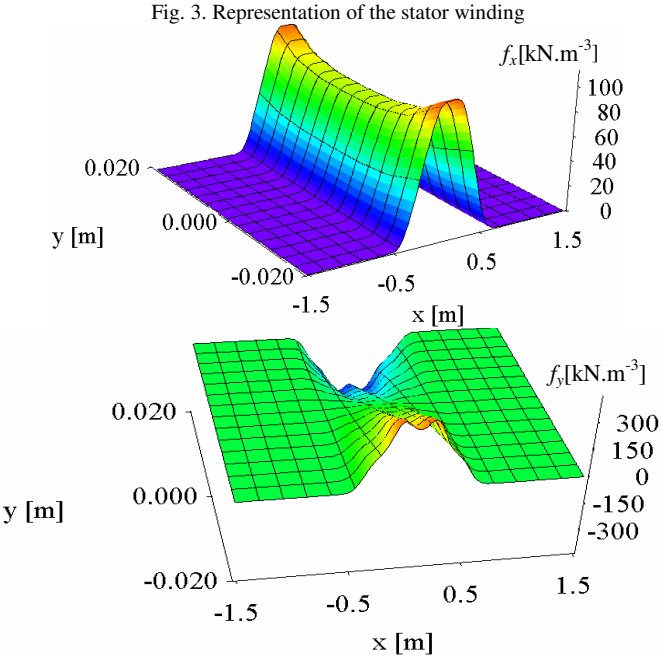

Fig. 4. Force density inside the secondary f_x and f_y at $v = 0$

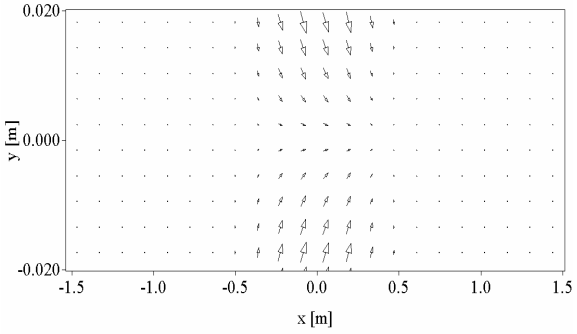

Fig.5 . Force density inside the secondary (vectorial representation ($v = 0$))

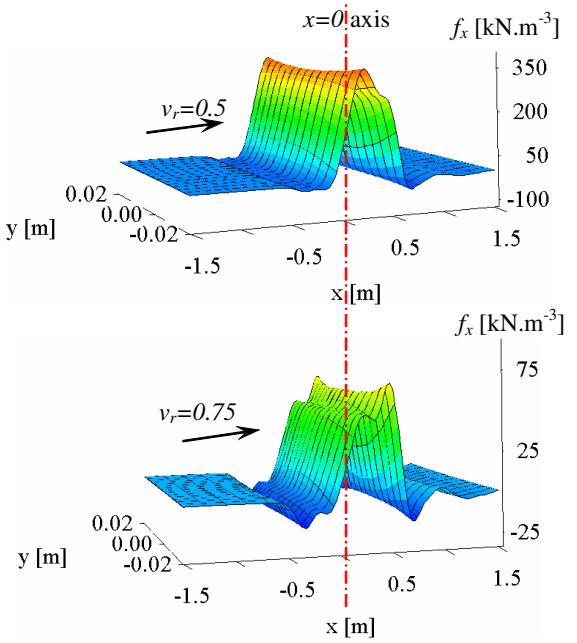

Fig. 6. Force density in the secondary f_x for different values of the speed

decomposition of the force field and to evaluate the rotational and gradient parts of the force [8]. This method is well described in [7] and gives a global view of the rotational and gradient component of the force field.

IV. Computation of the Hydraulic Pressure

The mean value of the hydraulic pressure can be given by:

$$-\frac{d\tilde{p}}{dx}(x)=\frac{1}{2\alpha}\int_{-\alpha}^{+\alpha} f_x(x,y)dy \tag{19}$$

So projection (19) on Hermite basis and using the projection of the mvp and its derivatives ((13) and (18)), we obtain:

$$-\frac{d\tilde{p}}{dx}(x)=\sum_{m,n=0}^{N}\psi_n(x)\,\psi_m(x)\,\varphi_{nm} \tag{20}$$

where: $\varphi_{nm}=\dfrac{\sigma}{2\alpha}\int_{-\alpha}^{+\alpha}\omega\Im\left[\overline{\alpha}_n(y)\,\gamma_m^*(y)\right]\nu\,\Re\left[\overline{\gamma}_n(y)\,\gamma_m^*(y)\right]dy$

This equation is continuous in the *y*-direction, but the coefficients $\overline{\alpha}_n(y)$ and $\overline{\gamma}_n(y)$ are known in their discreet form $\overline{\beta}_m^i$ and $\overline{\gamma}_m^i$. The coefficients φ_{mn} are then computed using discreet integration along the *y*-direction. If we consider that the pressure is zero enough far from the right end of the device, on can determine the evolution of the pressure along the channel (secondary) containing the liquid metal:

$$P(x)=\int_{-\infty}^{x}\frac{d\tilde{p}}{d\tau}(\tau)\,d\tau \tag{21}$$

Thanks to the ortogonality of the ψ_n, the total pressure is:

$$\Delta P=\lim_{x\to\infty}P(x)=\int_{-\infty}^{+\infty}-\frac{d\tilde{p}}{dx}(x)\,dx=\sum_{n=0}^{N}\varphi_{nn} \tag{22}$$

This expression gives the total pressure acting on the liquid metal and its is equal to the total force along the *x*-direction over the cross section of the channel. This same force can be computed in the motionless domain like in [5]. Figure 7 shows the evolution of the pressure along the *x*-direction for different values of the relative speed. The maximum values of $P(x)$ correspond to ΔP. One can see the highest value of ΔP is obtained for $v_r=0.25$. The stand still ($v_r=0$) value of the pressure is to weak.

V. Conclusion

A model of linear induction pumps is developed by using a coupled method combining finite element analysis and Fourier transform. The connection of the two methods is performed by a projection on Hermite basis that is invariant with respect to Fourier transform. The force density inside the secondary is determined and analyzed according to the changes made on the power supply and the velocity. A visualization of the fields leads to appreciate the effect of the velocity on the force distribution inside the channel. The use of Hermite orthogonal basis is very powerful and allows determining the performances by simplified expressions.

References

[1] G. W. Mclean, "Review of recent progress in linear motors", IEE Proceeding, Pa rt B., pp. 380-416, 1988.

[2] H. de Gersem, K. Hameyer, "Air-gap flux splitting for the time-harmonic finite elements simulation of single phase induction machines", *IEEE Trans. Mag.*, vol. 38, no. 2, 2002, pp. 1221-1224.

[3] E. Vassent, G. Meunier, J. C. Sabonnadière, "Simulation of induction machines using complex magnetofynamic finite elements", *IEEE Trans. Mag.*, vol. 25, no. 4, July 1989, pp. 3064-3066.

[4] S. Mezani, B. Laporte, N. Takorabet, "Complex finite element computation of induction motors with consideration of space harmonics", *IEEE International Electric Machines and Drives Conference IEMDC'03*, vol. 1, pp. 264–268, June 2003, Madison USA.

[5] B. Laporte, N. Takorabet, G. Vinsard, "An approach to optimize winding design in linear induction motors", *IEEE Transactions on Magnetics*, vol. 33, no. 2, March 1997, pp. 1844-1847.

[6] N. Takorabet, B. Laporte, G. Vinsard, "On the optimization of linear induction devices ", *Electrical Engineering –Archiv für Elektrotechnik* , vol. 80, pp. 221-226, Springer-Verlag 1997

[7] G. Vinsard, B. Laporte, N. Takorabet, J.P. Brancher "An analysis of the rotational forces in the secondary of an electromagnetic pump", *IEEE Trans. Mag.*, vol. 34, no. 5, September 1998, pp. 3552-3555

[8] A. Bossavit, "Magnetostatic problems in multiply connected regions : some properties of the curl operator", *IEE Proceedings Pt. A*, vol. 135, no.3 pp. 179-187, March 1988.

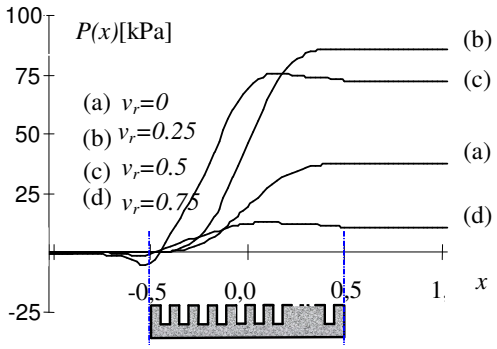

Fig. 7. Evolution of the pressure long the channel for different speeds.